Journal of Catalysis **185,** 199–212 (1999)
Article ID jcat.1999.2492, available online at http://www.idealibrary.com on IDEAL®

The Relationship between the Structure of NiMo/SiO_2 Catalyst Precursors Prepared in the Presence of Chelating Ligands and the Hydrodesulfurization Activity of the Final Sulfided Catalysts

Riccardo Cattaneo, Takafumi Shido, and Roel Prins[1]

Laboratory for Technical Chemistry, Federal Institute of Technology (ETH), 8092 Zürich, Switzerland

Received January 8, 1999; revised March 17, 1999; accepted March 17, 1999

The structure of nickel and molybdenum in silica-supported NiMo catalyst precursors, modified by the addition of various chelating ligands, was studied by means of X-ray, Raman, and UV–VIS spectroscopy. Thiophene hydrodesulfurization tests showed that a wide variety of ligands have a beneficial effect on the performance of the sulfided catalysts. The activity of catalysts prepared with nitrilotriacetic acid (NTA) and ethylenediamine (EN) was measured as a function of the ligand to Ni ratio in the catalyst precursors as well. EN gradually causes an improvement of the catalytic activity when the EN/Ni molar ratio increases from 0 to 4, while the best result for NTA is obtained when the NTA/Ni ratio is 1.5. UV–VIS spectra of NiMoEN impregnation solutions and dried catalysts showed that some EN is removed from the first coordination sphere of Ni during the drying procedure. Ni *K*-edge extended X-ray absorption fine structure (EXAFS) proved the presence of a Ni–Si shell and, thus, of Ni–SiO_2 interactions in the catalyst precursors prepared without ligands. These interactions disappeared gradually with increasing amounts of the ligand. Raman spectroscopy and Mo *K*-edge EXAFS showed that Mo is present on the support as a mixture of MoO_4^{2-} and polymolybdate clusters. Raman spectroscopy also suggested that these polymolybdate clusters interact with the support. Mo *K*-edge EXAFS spectra showed that EN has very little effect on Mo, whereas at NTA concentrations higher than 1 the $[MoO_3(NTA)]^{3-}$ complex is formed. The increase in activity obtained with EN and NTA is attributed to the elimination of Ni–SiO_2 interactions and to the presence of the ligands in the Ni coordination sphere, whereas the decrease in activity observed in catalysts with NTA/Ni ratios above 2 is explained by the formation of $[MoO_3(NTA)]^{3-}$.

Key Words: **hydrodesulfurization; nickel; molybdenum; silica; EXAFS; Raman; UV–VIS spectroscopy; chelating ligands.**

INTRODUCTION

Supported nickel- or cobalt-molybdenum sulfide catalysts are used extensively in the hydrotreatment of petroleum feedstocks. The increasing demand for efficient removal of sulfur, nitrogen, and metal contaminants has made it even more important to clarify the structure and the related catalytic activity of these complex catalyst systems. Molybdenum is considered to be the active ingredient, whereas Ni and Co are viewed either as promoters or as active sites. γ-Al_2O_3 is the most widely used support for such catalysts. Silica-supported Ni(Co)Mo catalysts show lower activities mainly because of the weaker interactions between the metals and the support, resulting in a relatively low dispersion of the metal sulfides on SiO_2. For this reason, few studies of the structure of Ni and Mo on SiO_2 have been published. The most stable Mo species on the silica surface with an isoelectric point of 2 are polymolybdates $[Mo_7O_{24-m}(OH)_m]^{(6-m)-}$ (1, 2), although Raman studies suggest the presence of interactions with the support and the formation of molybdosilicic acid (2, 3). Nickel can interact with silica to form Ni phyllosilicates (4, 5). This was, however, seldom observed for Ni/SiO_2 samples prepared by the classical incipient wetness impregnation method (6).

The addition of chelating ligands, such as nitrilotriacetic acid (NTA) or ethylenediamine tetraacetic acid (EDTA), to the impregnating solution has a beneficial effect on the catalytic activity of NiMo/SiO_2 catalysts (7–11). The resulting catalysts are even more active than alumina-supported catalysts. The improved activity has been ascribed to a better dispersion of nickel and molybdenum on the support in the catalyst precursors and, in the case of NTA, to the delayed sulfidation of Ni (12). Both factors would enhance the formation of the so-called Ni–Mo–S type II phase, which, at present, is considered to be the active phase in hydrotreating catalysts (9, 13, 14).

Previous work in our group concentrated on the effect of NTA on Ni and Mo in the impregnating solutions and in the catalyst precursors. It was found that NTA preferentially complexes Ni and causes a delay in its sulfidation (1, 12). To extend this work, the present study investigates the effect of other chelating ligands, especially ethylene

[1] To whom correspondence should be addressed. Fax: +41-1-6321162. E-mail: prins@tech.chem.ethz.ch.

0021-9517/99 $30.00

diamine, on $NiMo/SiO_2$ catalyst precursors and gives a more detailed structural description of the metal ions on the support. The structure of the catalyst precursors is correlated with the catalytic activity of the final sulfided catalysts in the hydrodesulfurization of thiophene at atmospheric pressure. The explanation of the structure of the oxidic precursors helps to understand the factors that influence the formation of active sites on the support during sulfidation. In particular, the structural changes in the catalyst precursors are revealed by means of extended X-ray absorption fine structure (EXAFS) and by UV–VIS and Raman spectroscopy as a function of the concentration of two chelating ligands, ethylenenediamine (EN) and nitrilotriacetic acid (NTA). In a subsequent publication, we will describe the sulfidation process of Ni and Mo and the characterization of the sulfided catalysts (15).

EXPERIMENTAL METHODS

Sample Preparation and Characterization

All catalysts were prepared by pore volume impregnation with a solution prepared by dissolving the organic complexing ligand in 15 ml of a 25% aqueous ammonia solution (Fluka puriss. p.a.), adding 3.60 g MoO_3 (25 mmol Fluka puriss. p.a.), and heating the solution to 80°C in order to dissolve MoO_3 (1). After cooling to about 60°C, 2.18 g $Ni(NO_3)_2 \cdot 6(H_2O)$ (7.5 mmol, Fluka purum p.a.) was added and dissolved. At this point the solution turned from uncolored to the color typical for the formed Ni complex, which was varying from blue to dark violet depending on the concentration and the kind of ligand employed. The pH was then adjusted to 8.0 with a 2 M HNO_3 solution and the solution was diluted to 25 ml with deionized water.

Several chelating ligands were tested. The investigated catalyst precursors are listed in Table 1. In all cases, the support was SiO_2 (C560 Chemie Uetikon), which had a particle size of 125–250 μm, a BET surface of 565 m^2/g, a BET pore volume of 0.83 ml/g, and which had been dried overnight at 120°C prior to impregnation. After impregnation the wet powder was again dried overnight at 120°C with a heating rate of 2°C/min. To avoid the destruction of the metallorganic complexes in the catalyst precursors before the sulfidation, no calcination was carried out at higher temperatures.

UV–VIS reflectance measurements were carried out on a Perkin Elmer Lambda 16 spectrometer, equipped with an integration sphere that allowed measurements in the reflection mode, using pure SiO_2 as a reference. Solutions were measured in 1-cm quartz cells. The Ni^{2+} concentration in the analyzed solutions was 0.03 mol/L; therefore the impregnating solutions had to be diluted.

The Raman measurements were performed on a Bruker Equinox 55 spectrometer equipped with a FT-Raman-Modul FRA 106, with a Nd : YAG laser (1064 nm), a CaF_2 beamsplitter, and a Ge detector (D418-S) cooled by liquid nitrogen. About 10 mg of the samples was pressed into a hole (diameter 2 mm, depth 1.5 mm) on an aluminum disk (diameter 1 cm). The number of accumulated spectra for each sample was 4096.

TABLE 1

$NiMo/SiO_2$ Catalysts Prepared with Different Chelating Ligands

Catalyst	Loading		n_L/Ni	log (K_1(NiL))
	Ni (%)	Mo (%)		
NiMo	1.4	7.5		
NiMo–nitrilotriacetic acid (NTA)	1.3	7.2	4	11.5
NiMo–EDTA	1.3	7.0	6	18.0
NiMo–ethylenediamine (EN)	1.3	6.9	2	7.5
NiMo–diethylenetriamine (DT)	1.3	7.0	3	10.7
NiMo–triethylenetetraamine (TT)	1.3	7.2	4	14.0
NiMo–tetraethylenepentamine (TP)	1.3	6.9	5	17.8
NiMo–pentaethylenehexamine (PH)	1.3	7.3	6	19.3
NiMo–18-crown-6	1.3	7.3	3	
NiMo–formic acid	1.3	7.1	1	0.5
NiMo–citric acid	1.3	7.2	4	4.2

Note. Molar ratio Ni : Mo : ligand = 0.3 : 1 : 0.3.

Sulfidation and Reaction

The oxidic precursors were sulfided at 400°C (heating rate 6°C/min) for 2 h with a mixture of 10% H_2S in H_2 (Messer Griesheim 3.0) that flowed through the reactor from the beginning of the heating process. The activity of all catalysts was tested in the hydrodesulfurization of thiophene at 400°C (12). The feed, consisting of 3% thiophene in H_2, was obtained by bubbling H_2 through a series of four thiophene saturators that were cooled to 2°C. The product stream was analyzed on line with a HP5890 gas chromatograph. The sulfidation and thiophene HDS reaction occurred at atmospheric pressure in an apparatus that was a modified version of the flow system described in (9).

EXAFS Measurements

EXAFS spectra of several compounds were measured at the Ni and Mo *K*-edges. The data were collected at the Swiss Norwegian Beamline (SNBL, BM1) at the European Synchrotron Radiation Facility (ESRF), Grenoble, France. The electron energy and ring current were 6 GeV and 130–200 mA, respectively. At SNBL the incident X-rays are monochromated by a Si (111) channel-cut monochromator and harmonics are rejected by a gold-coated mirror. The X-ray intensity is monitored by ionizing chambers and

the estimated resolution is 1 eV at the Ni *K*-edge and 2 eV at the Mo *K*-edge. For measurements at the Ni *K*-edge, the chambers for measuring I_0 and I_t were 17 and 31 cm long, respectively, and were filled with pure nitrogen and a mixture of argon and nitrogen ($Ar/N_2 = 40/60$). The chambers used for measurements at the Mo *K*-edge were 17 and 62 cm long and filled with pure argon and a mixture of krypton and nitrogen ($Kr/N_2 = 25/75$), respectively. Some of the data were collected at the General Purpose Italian Line for Diffraction and Absorption (GILDA, ID8) at the ESRF (16).

The Ni *K*-edge spectra were divided into six regions: 7780–8300 eV (pre-edge), 8300–8370 eV (edge region), and the four post-edge regions (3–6.5, 6.5–10, 10–15, 15–17 $Å^{-1}$) between 8370 and 9433 eV. The collection times for the data points in each scan and each region were 1, 1, 2, 3, 4, and 4 s, respectively. As far as the Mo *K*-edge was concerned, the collection times for each data point in a scan were 1, 2, 2, 3, and 3 s for the intervals 19,454–19,954 eV (pre-edge), 19,954–20,164 eV (edge region), and the three 6.5–10, 10–15, 15–21 $Å^{-1}$ post-edge regions between 20,164 and 21,684 eV, respectively. The distance between the postedge data points was determined so that the difference in their *k* values was smaller than 0.05 $Å^{-1}$. Five scans were averaged for the Ni *K*-edge and three for the Mo *K*-edge.

Catalyst samples were pressed into self-supporting wafers and mounted in an *in situ* EXAFS cell (17). The thickness of the samples was chosen to adjust the total absorption to $\mu x = 4$ for the Ni *K*-edge (low Ni concentration) and the edge jump to 1 for the Mo *K*-edge. The sample was cooled to liquid nitrogen temperature for all measurements.

EXAFS Analysis

The program XDAP (version 2.1.5) was used to analyze and fit the data (18, 19). The pre-edge background was approximated by a modified Victoreen curve and the background was subtracted using a cubic spline routine. The spectra were normalized by the edge jump. The k^3-weighted, and in some cases k^1-weighted, EXAFS functions were Fourier transformed and fitted in *R*-space. The free parameters were interatomic distance, coordination number, Debye–Waller factor, and the correction of the edge energy. The errors of the parameters were statistically estimated using the random errors of the observed data. The goodness of fit was calculated for every model from the *k*- and the *R*-space fit range and the number of free parameters (20).

Reference spectra were calculated using Feff7 (21) for several cluster models that will be discussed in more detail. Crystallographic data were obtained from the Inorganic Crystal Structure Database (ICSD-CRYSTIN) and the Cambridge Structure Database (CSD).

RESULTS

Catalytic Activity

The activity of catalysts prepared with various chelating ligands (Table 1) was investigated. The ligands can be divided in three groups: the chelating amines, such as ethylenediamine (EN), diethylenetriamine (DT), triethylenetetraamine (TT), tetraethylenepentamine (TP), and pentaethylenehexamine (PH), the combined aminoacetic acid-containing complexes such as NTA and EDTA, the organic formic and citric acids, and the crown ether 18-crown-6 (CE). All amines form very stable Ni complexes (22). In a Ni–CE complex, reported by Larson *et al.*, Ni coordinates three of the six oxygen atoms of the organic complex (23). The stability constants of the Ni complexes of formic acid and citric acid are lower than those of the amines (Table 1) (22). Attempts to use oxalic acid were abandoned because of the low solubility of nickel oxalate.

The results of the hydrodesulfurization measurements of thiophene at atmospheric pressure are presented in Fig. 1. The Ni : Mo : ligand molar ratio was 0.3 : 1 : 0.3 in all catalyst precursors. Catalysts prepared with NTA and EDTA show the highest rate constants. The n_L/Ni column in Table 1 gives the number of coordinating ligand atoms available per Ni atom, taking into account all potential coordinating atoms and that the Ni/ligand ratio is 1 for all samples. The number of theoretically coordinating atoms of CE was set at three as suggested in (23).

The concentration of the complexing ligands was varied for two catalysts in order to follow their catalytic activity as a function of the composition of the coordination spheres around the two metals. NTA and EN were chosen because of their different structures and because of what is known about their complexing properties. In Fig. 2, the thiophene HDS rate constants of the obtained catalysts are plotted as a function of the ligand to Ni ratio. For NTA a dramatic increase in catalytic activity is observed for the ligand to Ni ratio between 0 and 1. A maximum is reached between NTA/Ni = 1.5 and NTA/Ni = 2; the catalytic activity decreases for higher NTA/Ni ratios. The activity of catalysts prepared with EN is generally lower but increases at first rapidly and then more gradually until EN/Ni = 4.

Characterization of Nickel

UV–VIS spectroscopy. UV–VIS spectra of the impregnating solutions and of several dried catalyst precursors were collected to investigate the coordination of the Ni^{2+} ions. Replacing coordinating oxygen atoms with nitrogen atoms shifts the VIS absorption bands in the region between 500 and 700 nm, attributed to the $^3A_{2g}(F)$ to $^3T_{1g}(F)$ transition, to lower wavelengths (24). Table 2 lists the wavelengths of this absorption band for aqueous solutions of $Ni(NO_3)_2 \cdot 6(H_2O)$ with different amounts of EN.

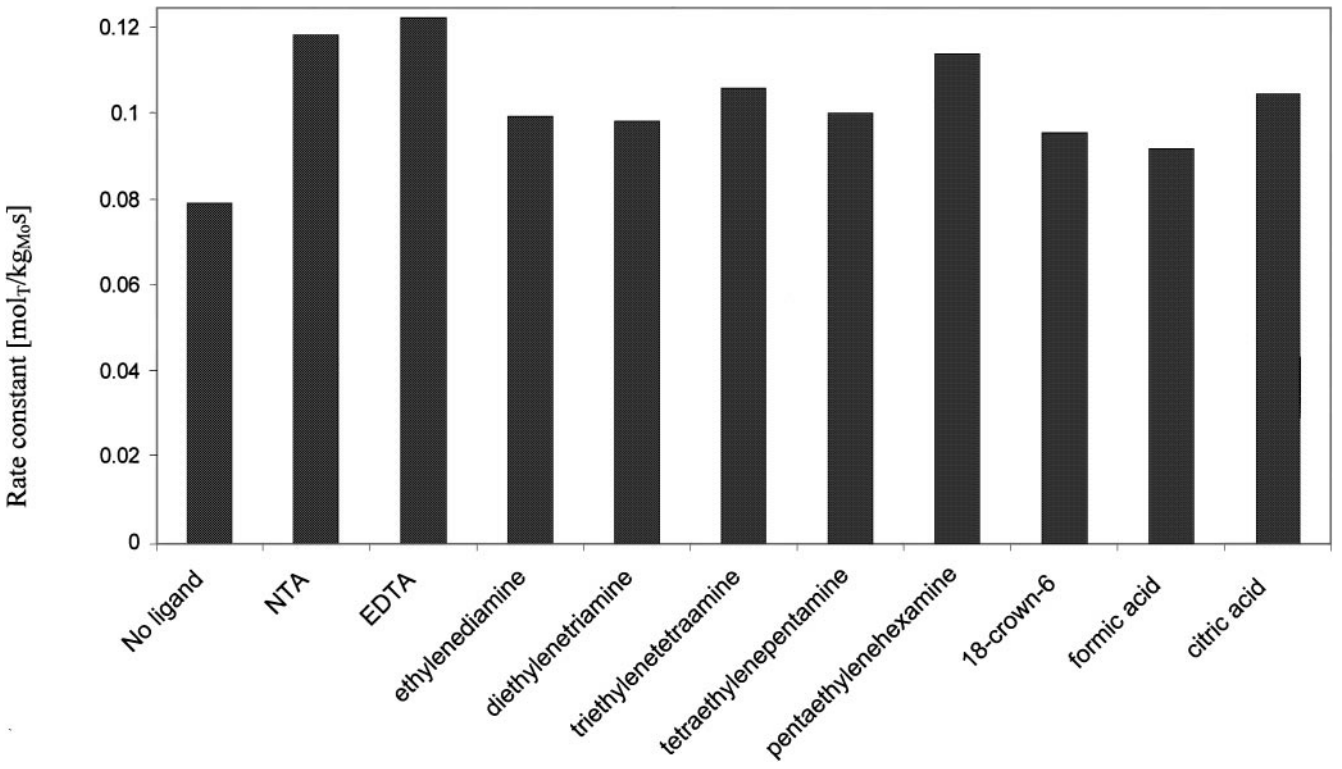

FIG. 1. Activity of $NiMo/SiO_2$ catalysts prepared by adding different ligands.

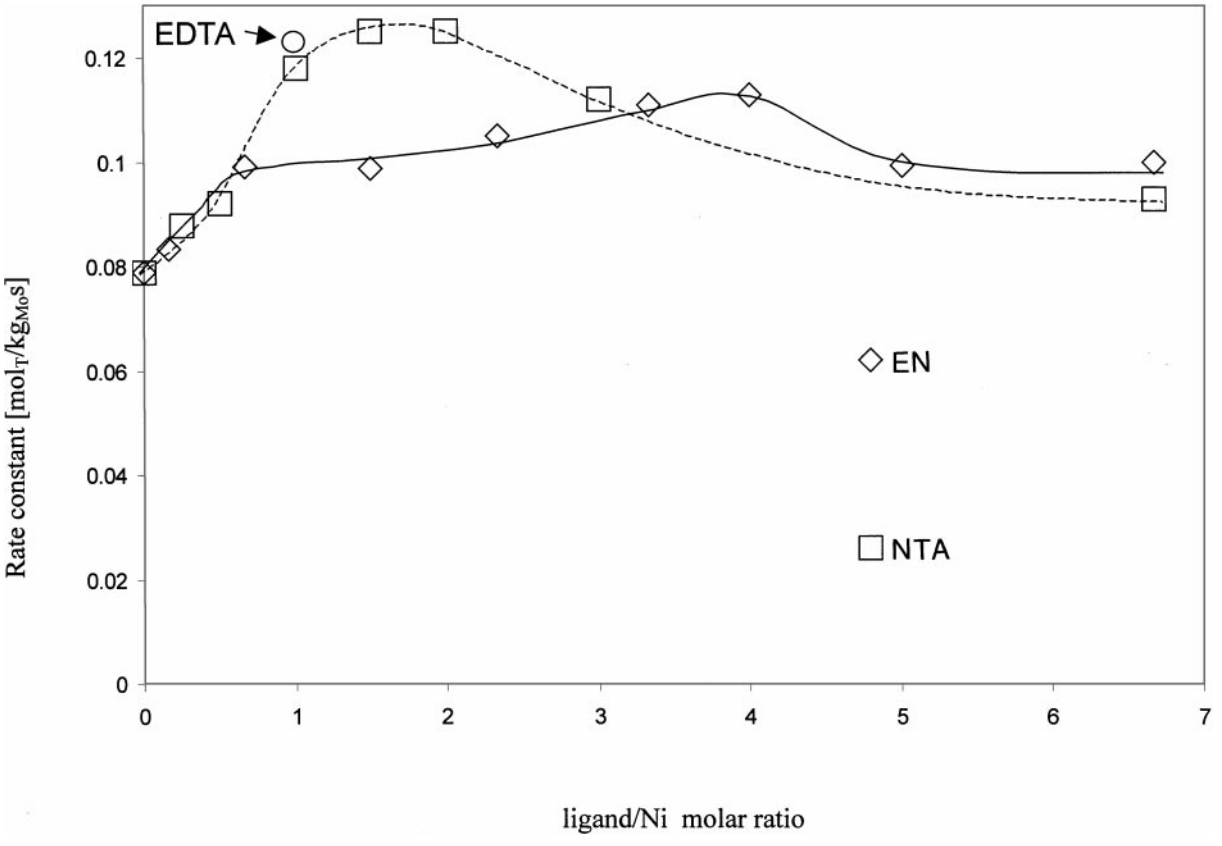

FIG. 2. Activity of $NiMo/SiO_2$ catalysts prepared with different amounts of ethylenediamine and nitrilotriacetic acid (Ni : Mo = 0.3 : 1).

TABLE 2

UV-VIS Absorption Bands of Ni–EN Complexes in Water and Ammonia Solutions

EN : Ni	In H_2O (nm)	In ammonia solution (8 M, pH 8.0) (nm)
0	723	608
1	618	595
2	565	562
3	545	546

The solutions were prepared in the presence and absence of NH_3. The absorption maxima of both solutions shift to lower wavelengths with increasing EN concentration. Those species that, according to thermodynamics, should be present in aqueous Ni–EN solutions were calculated from the stability constants of the Ni^{2+} complexes using an extended version of the program Spex (1, 25, 26). In the solution with EN/Ni = 1, 63% of Ni^{2+} should be present as $[Ni(EN)(H_2O)_4]^{2+}$, 20% as $[Ni(EN)_2(H_2O)_2]^{2+}$ and 17% as $[Ni(H_2O)_6]^{2+}$. Hence, in passing from the solution without EN to the solution with EN/Ni = 1, about one-third of the oxygen atoms of H_2O coordinated to Ni are replaced with nitrogen atoms of EN. This explains the large difference in the wavelength of the absorption bands of the two solutions. In the aqueous solution with EN/Ni = 2, about 85% of Ni^{2+} should be present as $[Ni(EN)_2(H_2O)_2]^{2+}$, whereas for EN/Ni = 3, $[Ni(EN)_3]^{2+}$ corresponds to 98% of all Ni^{2+} present in the solution.

The absorption maxima of the ammonia solutions have lower wavelengths than those of the aqueous solutions for EN/Ni = 0 and 1 but are practically the same for higher EN concentrations. This is due to the fact that when no EN is present in the solution, Ni^{2+} is present as 45% $[Ni(NH_3)_6]^{2+}$, 45% $[Ni(NH_3)_5(H_2O)]^{2+}$, and 10% $[Ni(NH_3)_4(H_2O)_2]^{2+}$. When EN is added to the solution, mixed Ni–EN–NH_3–H_2O complexes are formed.

The spectra of some NiMoEN impregnating solutions (Fig. 3) show that an increasing EN concentration affects the Ni^{2+} environment. In the regions around 850, 500–650, and 300–400 nm, the absorption bands shift to higher energies with increasing EN concentration. The absorption maxima for the bands in the region between 500 and 650 nm are listed in Table 3. Ammonia is present in the solutions; thus, the absorption maxima should be compared with those of the ammonia solutions in Table 2. The spectrum of the impregnating solution without EN has a maximum at 620 nm, whereas the Ni–NH_3 solution has a maximum at 608 nm. The impregnating solutions with the highest EN/Ni ratios (3.33, 6.66) show absorption bands with particularly low wavelengths. The presence of Mo explains this shift of the maxima, because it is the only parameter that is different to the ammonia solutions.

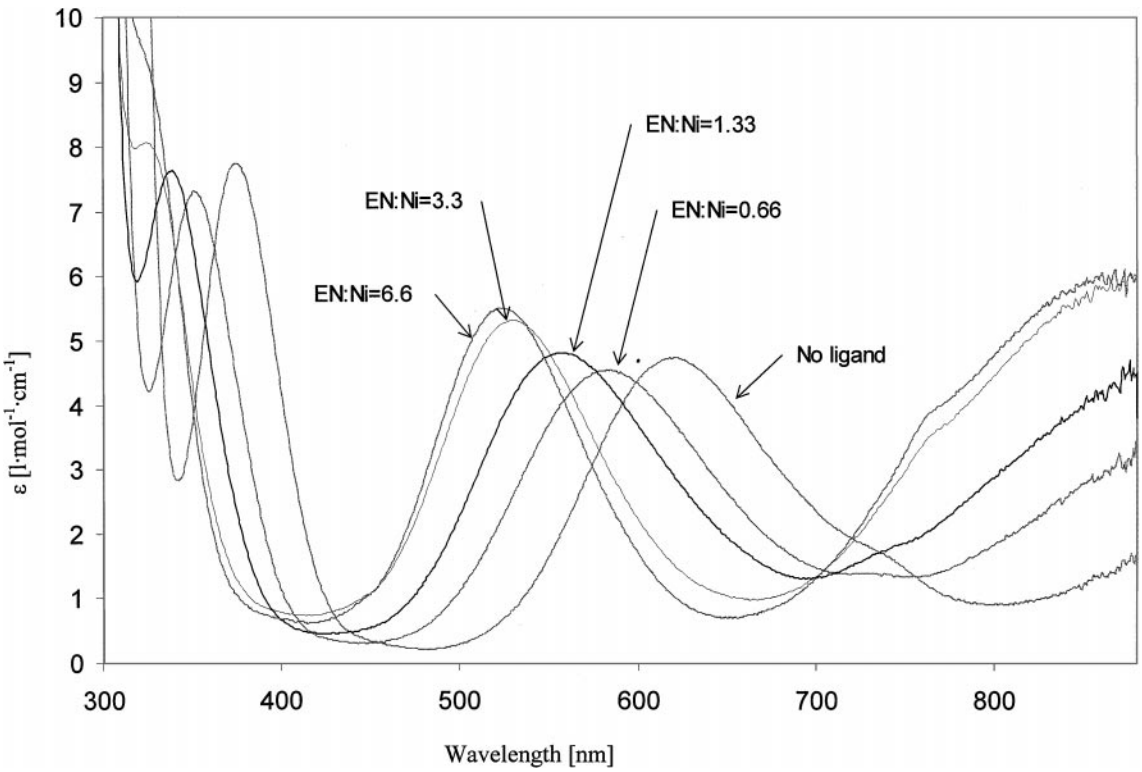

FIG. 3. UV–VIS spectra of NiMoEN impregnating solutions containing different amounts of ethylenediamine, $[Ni]_{tot} = 0.03$ mol L^{-1}, pH 8.

TABLE 3

UV-VIS Absorption Bands of the Impregnating Solutions (pH 8.0, Ni : Mo = 0.3 : 1) and of the Dried Catalyst Precursors

EN : Ni	Impregnating solutions (nm)	Dried catalyst precursors (nm)
0	620	708
0.16	594	709
0.66	583	710
1.33	557	659
3.33	530	585
6.66	523	549

The reflectance UV–VIS spectra of the dried catalyst precursors are presented in Fig. 4. Mo compounds on the support absorb very strongly below 500 nm, covering all signals arising from nickel in this region. Nevertheless, it is possible to distinguish an absorption band for each spectrum. The absorption maxima are listed in Table 3. From the data and the spectra, it is clear that, for the catalyst precursor without a ligand and for catalyst precursors with EN/Ni = 0.16 and 0.66, almost no Ni–amine complexes were present after drying. Some EN was apparently removed from the Ni^{2+} ions in the catalyst precursors with higher ligand concentrations (see Table 3), because the wavelengths of the absorption maxima for the dried catalyst precursors with EN/Ni = 1.33, 3.33, and 6.66 are higher than those for Ni^{2+} complexes containing the same number of amine ligands. The values for Ni–EN complexes in aqueous solutions (Table 2) suggest that the dried catalyst precursors with EN/Ni = 1.33, 3.33, and 6.66 contain less than 1, fewer than 2 and slightly fewer than 3 EN molecules per Ni^{2+} ion, respectively.

Ni XAS of NiMoEN/SiO_2. To follow the change in structure of the catalyst precursors as a function of the amount of ligand used during the preparation, we compared the Fourier transformed $\chi(k) \cdot k^3$ functions measured at the Ni *K*-edge for five different catalyst precursors: NiMo/SiO_2 and four NiMoEN/SiO_2 compounds with EN/Ni = 0.16, 0.66, 3.33, and 6.66.

The Ni *K*-edge Fourier transformed $\chi(k) \cdot k^3$ functions are shown in Fig. 5 (*k*-range, 3–14 $Å^{-1}$). The results of the fits are listed in Table 4. In the NiMo/SiO_2 spectrum, there are two main peaks at 1.6 and 3 Å (uncorrected for phases). The first is ascribed to the oxygen atoms that surround the Ni^{2+} ions. The reference for oxygen was produced with the Feff code using a Ni–O distance of 2.12 Å. The first shell of the catalyst precursors prepared with EN was analyzed with references for Ni–O and Ni–N references that were calculated with the Feff code, with distances and coordination numbers taken from the crystallographic data of the complex $Ni(EN)_2 \cdot 2H_2O$ (27). The first shell of the Ni^{2+} ions of the catalyst precursors with EN/Ni = 0.16 was fitted using an oxygen contribution only, since UV–VIS showed that

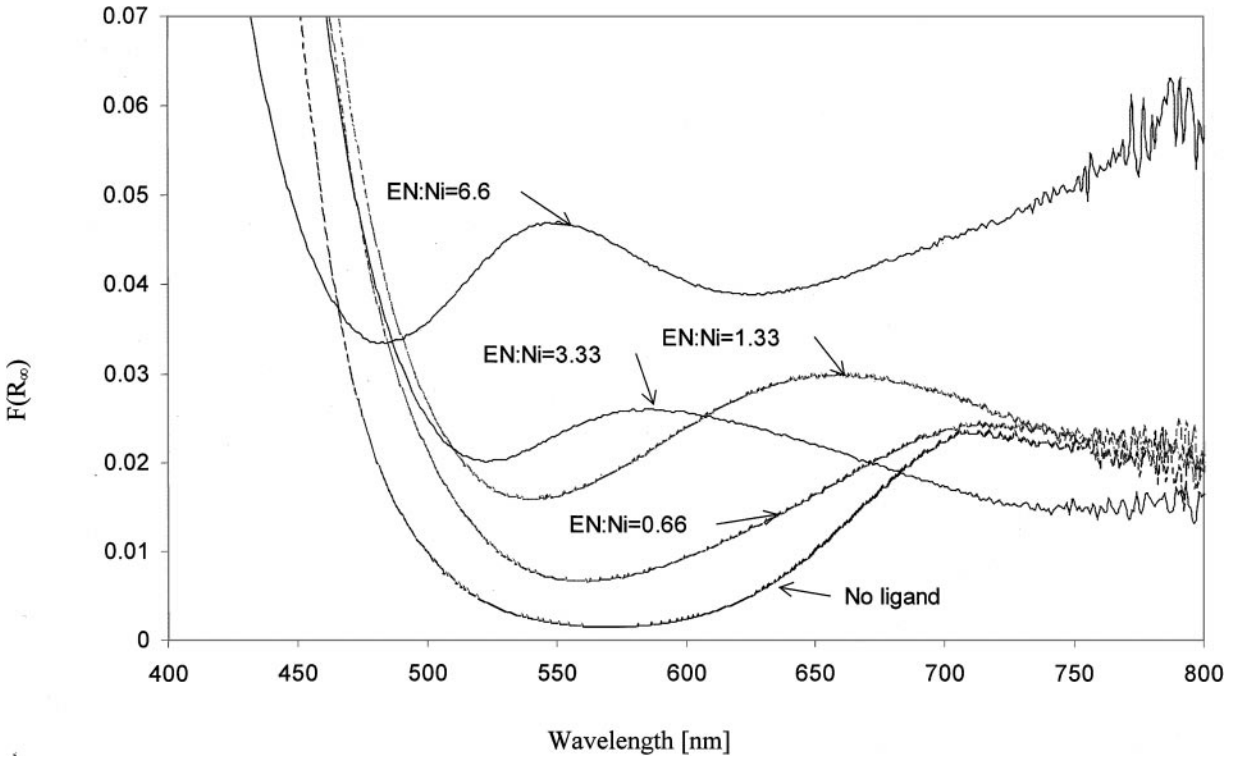

FIG. 4. Reflectance UV–VIS spectra of dried NiMo/SiO_2 precursor catalysts prepared with different amounts of ethylenediamine.

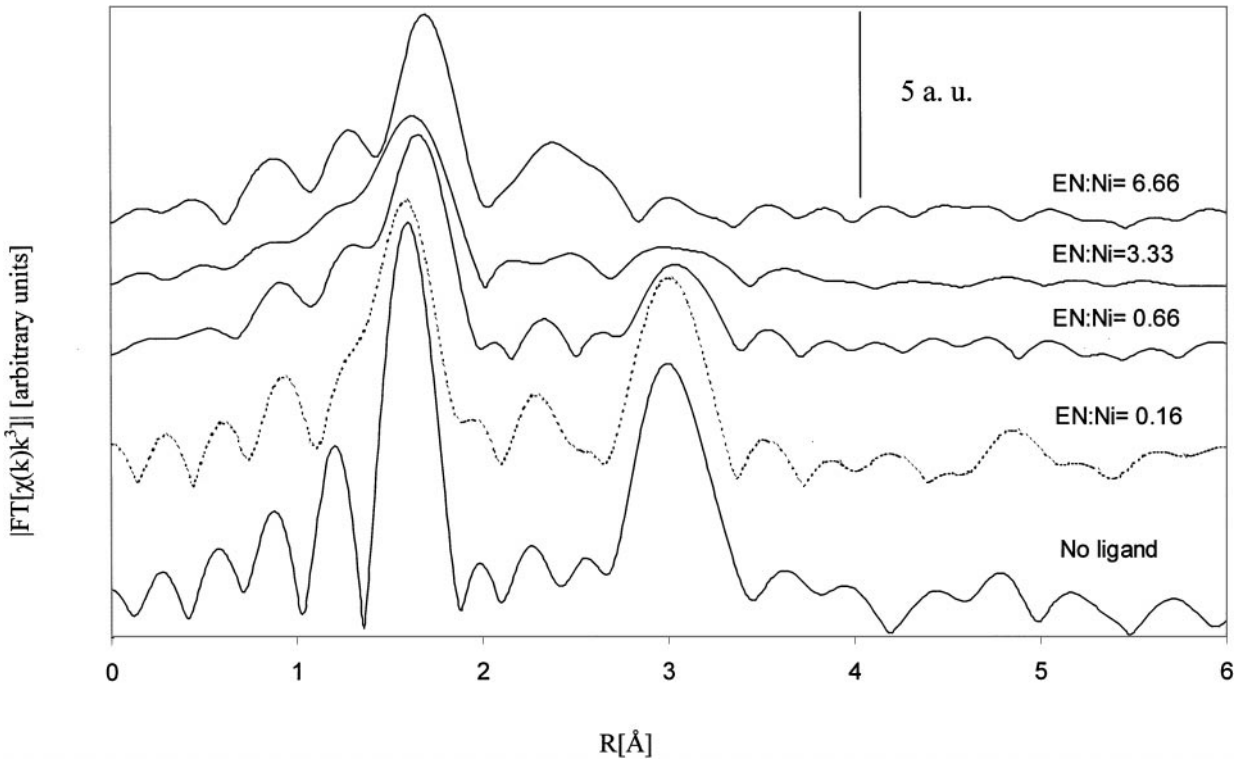

FIG. 5. Absolute parts of the Fourier transforms of the Ni *K*-edge $\chi(k) \cdot k^3$ EXAFS of NiMo/SiO_2 catalyst precursors as a function of the amount of ethylenediamine used during preparation.

no EN molecule is surrounding Ni in the catalyst precursor (see Table 3). In contrast, for the catalyst precursors with EN/Ni = 0.66 and 3.33, both the nitrogen and the oxygen contribution were used for the fitting. For the catalyst precursor with EN/Ni = 0.66, the coordination number for nitrogen is relatively low (0.2). For EN/Ni = 3.33, it was 3.7, whereas for oxygen it was 3.2. These results agree with the UV–VIS measurements that revealed Ni to be surrounded, on average, by fewer than one and two EN molecules for the catalyst precursors with EN/Ni = 0.66 and 3.33, respectively. Moreover, in the same spectrum, the features of a Ni–EN coordination become visible. The peak at 2.5 Å (not

TABLE 4

Structural Parameters Resulting from the Ni *K*-Edge Fourier-Filtered k^3-Weighted EXAFS Functions of the Dried NiMoEN/SiO_2 Catalyst Precursors Prepared with Different Amounts of Ethylenediamine

Catalyst precursor	Shell	$N_{coord.}$	R (Å)	$\Delta\sigma^2$ (10^{-3} Å^2)	ΔE_0 (eV)	Goodness of fit	R range (Å)
NiMo	O	4.40	1.99	−2.50	7.8	3.50	0.60–3.60
	Si	4.50	3.35	−2.91	4.7		
EN : Ni = 0.16	O	6.8	2.00	3.19	5.3	0.83	1.00–3.6
	Si	3.0	3.35	−3.85	−4.8		
EN : Ni = 0.66	N	0.2	1.82	−6.73	3.0	1.08	1.00–3.4
	O	6.4	2.03	3.83	3.7		
	Si	1.5	3.37	−3.63	−7.2		
EN : Ni = 3.33	N	3.7	2.03	1.10	0.8	1.50	1.00–3.40
	O	3.2	2.11	1.18	5.3		
	C	2.1	2.82	4.24	11.9		
	Si	0.8	3.37	−3.46	−7.7		
EN : Ni = 6.66	N	5.5	2.13	0.51	−1.5	2.09	1.20–2.90
	C	8.0	2.92	4.17	3.1		

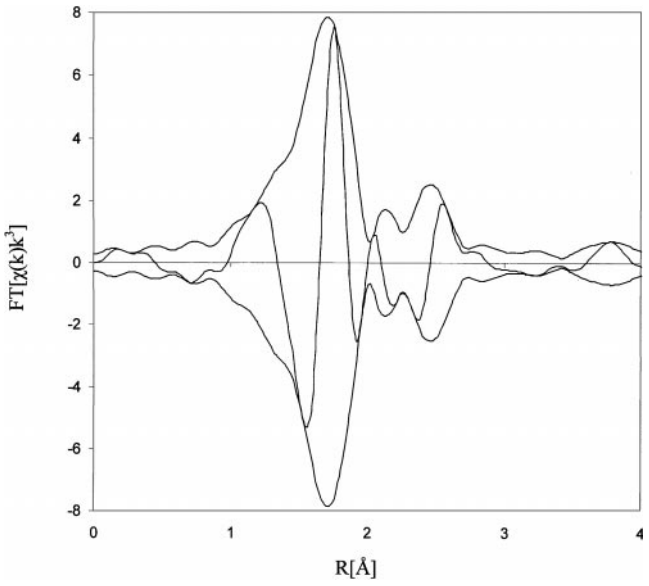

FIG. 6. Fourier transform of the $\chi(k) \cdot k^3$ EXAFS of $Ni(EN)_2 \cdot 2H_2O$ simulated by Feff7.

phase corrected) arises from the scattering of the carbon atoms of EN, as was seen in a Feff7 simulated spectrum (Fig. 6) of the complex $Ni(EN)_2 \cdot 2H_2O$ (27), from which we calculated the Ni–C reference. The small peak at 2.15 Å is caused by the interference of the signals of the nitrogen and oxygen atoms in the first shell. The Ni–C coordination number of 2.1 for the catalyst precursor with EN/Ni = 3.33 is, however, lower than expected, since it should equal the Ni–N coordination number (3.7). The greater distance from the central atom may explain the enhanced mobility of the carbon atoms and the resulting underestimation of the coordination number.

In the case of the catalyst precursor with an EN/Ni = 6.66, fitting with the Ni–O reference yielded a coordination number of only 4.1. With the Ni–N reference, in contrast, a coordination number of 5.5 was obtained, closer to the value of 6 for the expected octahedral geometry around nickel. The degrees of freedom were not sufficient to perform a fit using the Ni–N and the Ni–O contributions simultaneously. The second shell was fitted with a Ni–C contribution, but the resulting coordination number was 8, which is too large even for a $Ni(EN)_3$ complex. Moreover, the features of the fitting curve suggested that an additional contribution overlaps with that of Ni–C. Several attempts (Ni–Ni, Ni–Si, Ni–Mo) were made to identify the element responsible for the second contribution but with no success. From the UV–VIS spectra, the average number of EN molecules around Ni in the catalyst precursor with EN/Ni = 6.66 should be slightly smaller than 3. It is not possible to calculate the exact number of EN molecules coordinated by Ni by means of EXAFS, because the N and O atoms in the first shell cannot be distinguished, even though it is clear that nitrogen is the main contribution and the number of carbon atoms resulting from the fit is overestimated.

As far as the second shell is concerned, comparing the spectrum of $NiMo/SiO_2$ with the spectra of the catalyst precursors with EN/Ni = 0.16 and 0.66, there is a clear decrease in the intensity of the signal at 3.05 Å (not phase corrected). This is assumed to be generated by a Si shell of the support. Clause *et al.* (28) reported on Ni silicates in their Ni/SiO_2 compounds that were prepared by incipient wetness impregnation as well as by ion exchange. In their EXAFS spectra they observed signals mainly at 2.8 Å (not phase corrected) that they attributed to a combined contribution of Ni and Si. However, they measured all samples at room temperature. In contrast, in our spectrum, judging from the distance from the central atom, the peak at 3.05 Å is thought to arise exclusively from a Si contribution. Since the measurements were carried out at liquid nitrogen temperature, the contributions of the thermal vibrations are drastically reduced, enabling the detection of a *cleaner* signal of the backscatterer atoms. The reference for the Si shell was calculated with the Feff code using a Ni–Si distance of 3.3 Å. A fit with a Ni–Mo coordination was attempted, but the F-test showed that there is a 85% probability that the Ni–Si model describes the system better than the Ni–Mo shell. In the catalyst precursor with EN/Ni = 0.16, the Ni–Si coordination number decreases from 4.5 to 3.0. The signal of the Ni–Si shells becomes smaller, but also broader, with increasing amounts of EN, but it is still present at EN/Ni = 3.33, until it disappears at the highest EN concentration.

Ni XAS of NiMoNTA/SiO₂. The k^3-weighted Fourier transformed EXAFS functions of $NiMoNTA/SiO_2$ catalyst precursors with NTA/Ni = of 0.25, 0.66, 1.5, 3.0, and 6.66 (Fig. 7) show that NTA strongly affects the first and the second shells around Ni. The *k*-range of the presented data is 3–14 $Å^{-1}$ for the catalyst precursor without a ligand as well as for the precursors with NTA/Ni = 0.25, 1.5, 3.0, 6.66; it is 3–10 $Å^{-1}$ for the catalyst precursor with NTA/Ni = 0.66. The second signal at 2.3 Å (not phase corrected) arises from the carbon atoms of NTA. The results of the fits (Table 5), with the exception of the precursor catalyst with NTA/Ni = 1.5, clearly show that the Ni–C coordination number increases gradually with increasing amount of NTA. For the catalyst precursor with NTA/Ni = 0.25 the signal was too weak to be fitted. On the contrary, for NTA/Ni = 1.5, the coordination number obtained by the fit of the Ni–C shell was too large (9.0), as in the case of the catalyst precursor prepared with ethylenediamine with EN/Ni = 6.66 (see above). For NTA/Ni = 0.66, the average Ni–C coordination number is only 0.9, while it increases to almost 5 and 6 when the ratio is 3.33 and 6.66, respectively. In fact, if it is assumed that all NTA present binds to Ni and that Ni is complexed by the three acetate arms of the chelating agent, then the Ni–C coordination

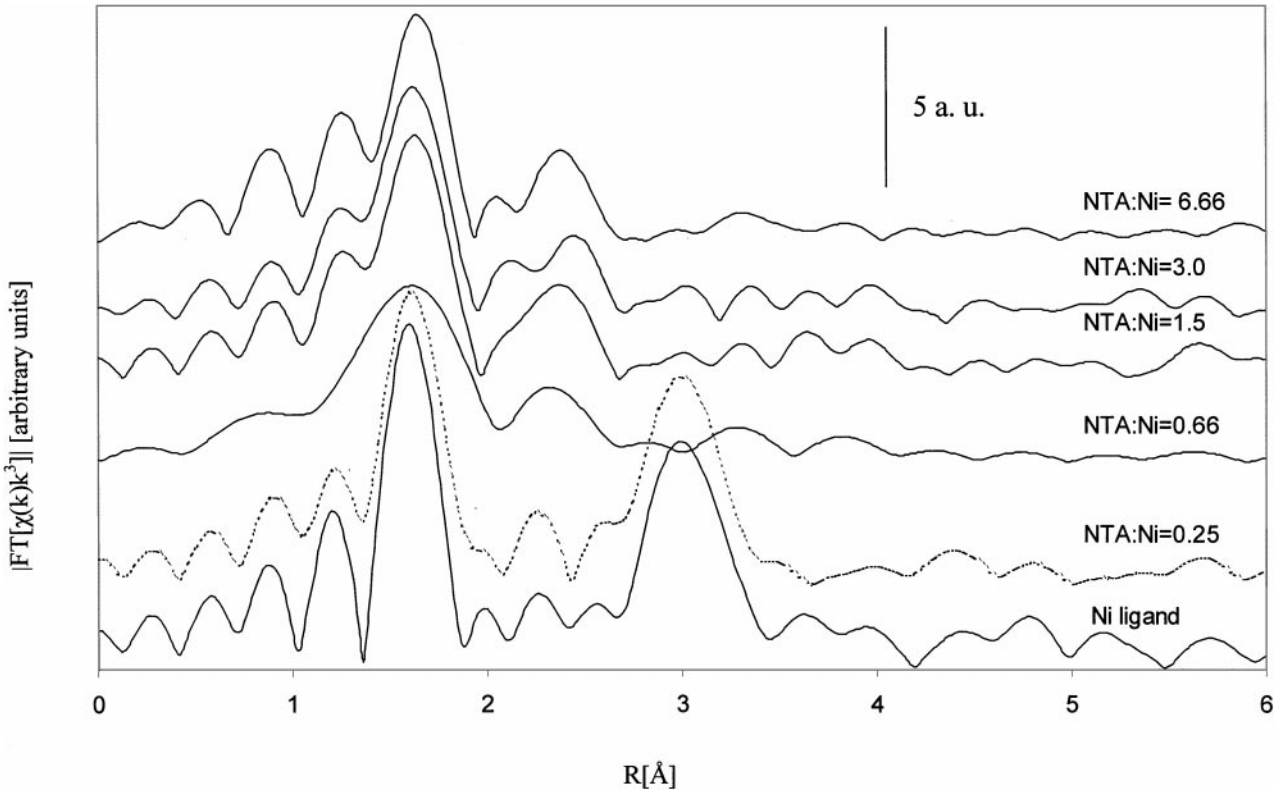

FIG. 7. Absolute parts of the Fourier transforms of the Ni *K*-edge $\chi(k) \cdot k^3$ EXAFS of NiMo/SiO_2 catalyst precursors as a function of the amount of nitrilotriacetic acid used during preparation (*k*-range 3–14 Å, except NTA : Ni = 0.66, *k*-range 3–10 Å).

number should be 3.9 for NTA/Ni = 0.66 and 6 for NTA/Ni = 1. Two explanations for such a low Ni–C coordination number are that the nickel ions exchanged some of the ligand bonds for interactions with the support and are coordinated by only two of the three acetate arms and by the nitrogen atom of the NTA molecules, or that a fraction of the nickel is present on the support in another structure. When NTA/Ni = 6.66, the Ni–C coordination number is about 6, suggesting that all Ni atoms are completely complexed by one NTA molecule.

The Ni–Si contribution at 3.05 Å (not phase corrected) is still present for the catalyst precursor with the lowest NTA concentration but is not detected at higher NTA concentrations.

TABLE 5

Structural Parameters Resulting from the Ni *K*-Edge Fourier-Filtered k^3-Weighted EXAFS Functions of the Dried NiMoNTA/SiO_2 Catalyst Precursors Prepared with Different Amounts of NTA

Catalyst precursor	Shell	$N_{coord.}$	*R* (Å)	$\Delta\sigma^2$ (10^{-3} Å^2)	ΔE_0 (eV)	Goodness of fit	*R* range (Å)
NiMo	O	4.40	1.99	−2.50	7.8	3.50	0.60–3.60
	Si	4.50	3.35	−2.91	4.7		
NTA : Ni = 0.25	O	5.9	2.02	0.53	4.0	1.69	1.00–3.60
	Si	3.1	3.35	−4.19	−4.0		
NTA : Ni = 0.66	O	5.8	2.05	1.44	2.9	4.33	1.00–3.00
	C	0.9	2.86	−13.82	9.5		
NTA : Ni = 1.50	O	6.0	2.04	1.45	1.8	4.1	1.00–2.70
	C	9.0	2.83	2.03	−2.0		
NTA : Ni = 3.00	O	5.7	2.04	0.84	4.1	1.62	1.00–2.70
	C	4.8	2.87	−0.78	3.6		
NTA : Ni = 6.66	O	5.1	2.05	0.70	2.8	2.75	0.60–2.80
	C	5.9	2.84	1.45	8.0		

Characterization of Mo

Laser Raman spectroscopy. Raman spectra were recorded for dried catalyst precursors. The spectra of SiO_2-supported Mo, NiMo, and NiMoEN (EN/Ni = 0.16, 0.66) are presented in Fig. 8. Catalyst precursors containing NTA and higher EN concentrations could not be investigated by Raman, because the samples were destroyed by the laser beam. The spectra show common features arising from silica (bands at 485, 217 cm^{-1}) and from the NO_3^- ion (710 cm^{-1}). The bands at 973, 955, and 616 cm^{-1} in the spectrum of the sample containing only Mo correspond in wave number to β-molybdosilicic acid (3), a Keggin type structure consisting of 12 octahedral MoO_6 units surrounding a SiO_4 tetrahedron (29). However, the high intensity of the band at 955 cm^{-1} and the presence of the band at 367 cm^{-1} and the shoulder at 238 cm^{-1} suggest that polymolybdates are also present on SiO_2. The mentioned Raman bands are consistent with octahedrally coordinated polymolybdates interacting weakly with the silica surface, similar in structure to the aqueous isopolymolybdate anions $Mo_7O_{24}^{6-}$ and $Mo_8O_{26}^{4-}$ (2, 30). Several aqueous isopolymolybdate anions composed of edge sharing MoO_6 octahedra display an intense Mo–O symmetric stretching vibration from 943 to 965 cm^{-1} (31, 32). Moreover, the weak shoulders at 900 and 315 cm^{-1} evidence the presence of molybdates in this supported material.

A band at 961 cm^{-1} is visible in the spectrum of the NiMo/SiO_2 sample, similar to the 955 cm^{-1} isopolymolybdate band in the Mo-only sample. Nevertheless, the signals at 905 and 315 cm^{-1} are characteristic for MoO_4^{2-} (32–35). As a consequence, in the absence of a ligand, Mo is present on the support as a mixture of polymolybdate clusters and isolated MoO_4^{2-} molecules.

In the spectra of catalyst precursors prepared with EN a shoulder around 900 cm^{-1}, typical of MoO_4^{2-}, was also observed. The two bands at 960 and 940 cm^{-1} are, nevertheless, the most intense signals. It is difficult to say whether both bands or just one arises from polymolybdate species. The weak signal at 360 cm^{-1} is a further proof that such clusters are present. Polyanions in aqueous solutions and supported on silica show a band around 960 cm^{-1} (2, 30), whereas for crystalline $(NH_4)_6Mo_7O_{24} \cdot 4H_2O$ and $(NH_4)_6Mo_2O_7$ the band shifted to 937 cm^{-1} (36). This suggests that two kinds of Mo polyanions are present in the samples prepared with EN: one which forms weak

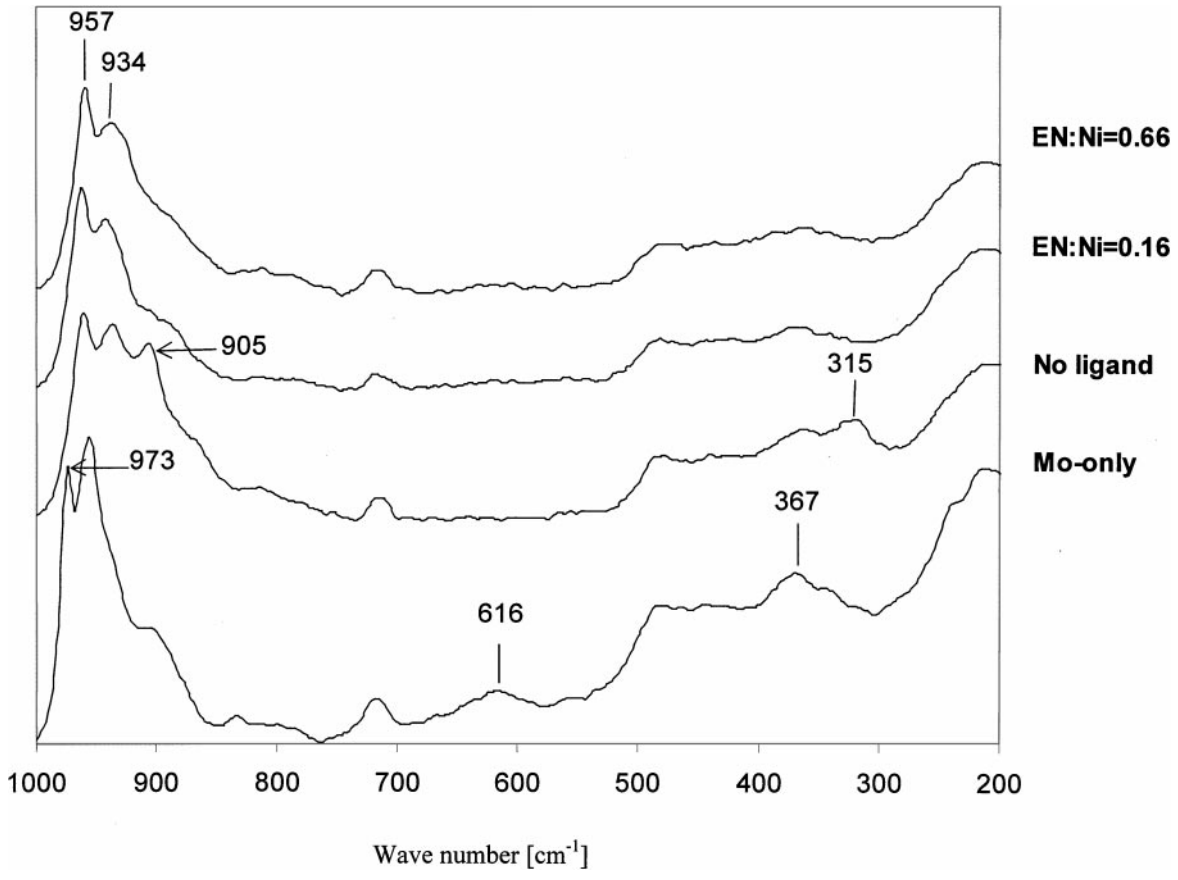

FIG. 8. Raman spectra of SiO_2-supported catalyst precursors.

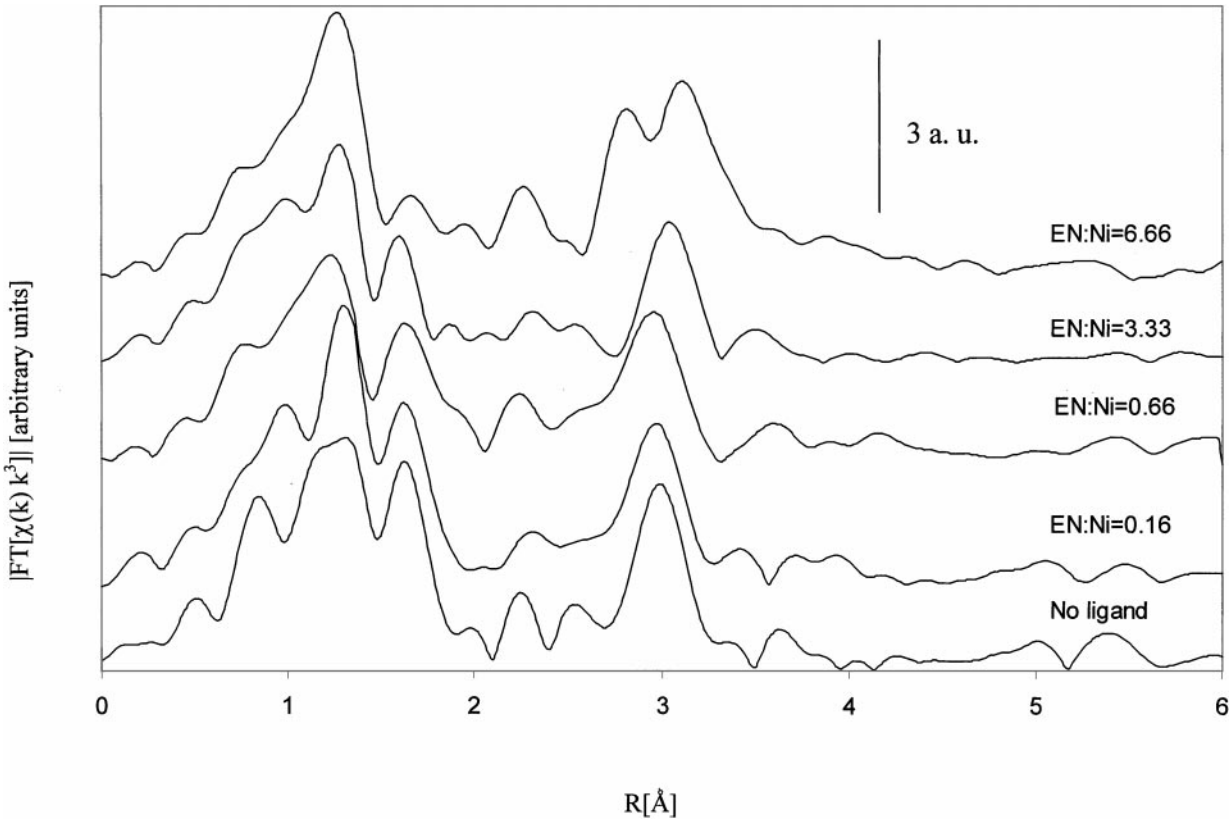

FIG. 9. Absolute parts of the Fourier transforms of the Mo *K*-edge $\chi(k) \cdot k^3$ EXAFS of NiMo/SiO_2 catalyst precursors as a function of the amount of ethylenediamine used during preparation (k-range 3–17 $Å^{-1}$).

interactions with SiO_2 and the other which is like the crystalline compound and is not influenced by the support.

Mo XAS of NiMoEN/SiO_2. Figure 9 shows the Fourier transformed k^3-weighted EXAFS functions of NiMo/SiO_2 and NiMoEN/SiO_2 catalyst precursors with EN/Ni = 0.16, 0.66, 3.33, and 6.66. The results of the fits are presented in Table 6. We did not fit the Mo–O shells, because the overlapping Mo–O contributions at different distances cause a reduction in the signals, with consequent underestimation of the coordination numbers (37). The signal at 3 Å, due to the backscattering of the first Mo–Mo shell, was fitted with 0.9 Mo–Mo contributions for the catalyst precursor without a ligand. The Mo–Mo coordination number increases to 1.3 for the catalyst with EN/Ni = 0.66. The Mo–Mo contribution is more intense and narrower for the catalyst precursor prepared without a ligand than for the catalyst precursors prepared with EN; the Mo–Mo coordination number, however, is comparable. This is a sign of a better defined distance of the Mo–Mo shell. The signal splits into two parts in the spectrum of the catalyst precursor with EN/Ni = 6.66, suggesting that the structure of the second shell in this compound is more complex than those in the other catalyst precursors. A fit with two

TABLE 6

Structural Parameters Resulting from the Mo *K*-Edge Fourier-Filtered k^3-Weighted EXAFS Functions of the Dried NiMoEN/SiO_2 Catalyst Precursors Prepared with Different Amounts of Ethylenediamine: Nearest Mo Shell

Catalyst precursor	Shell	$N_{coord.}$	R (Å)	$\Delta\sigma^2$ (10^{-3} Å^2)	ΔE_0 (eV)	Goodness of fit	R range (Å)
NiMo	Mo	0.9	3.29	−0.81	6.0	2.39	2.70–3.30
EN : Ni = 0.66	Mo	1.3	3.30	0.90	7.2	2.35	2.70–3.30
EN : Ni = 3.33	Mo	1.0	3.36	0.33	3.0	3.68	2.75–3.35
EN : Ni = 6.66	Mo	0.5	3.16	−1.65	15.6	4.09	2.60–3.60
	Mo	0.4	3.42	−4.20	−3.9		

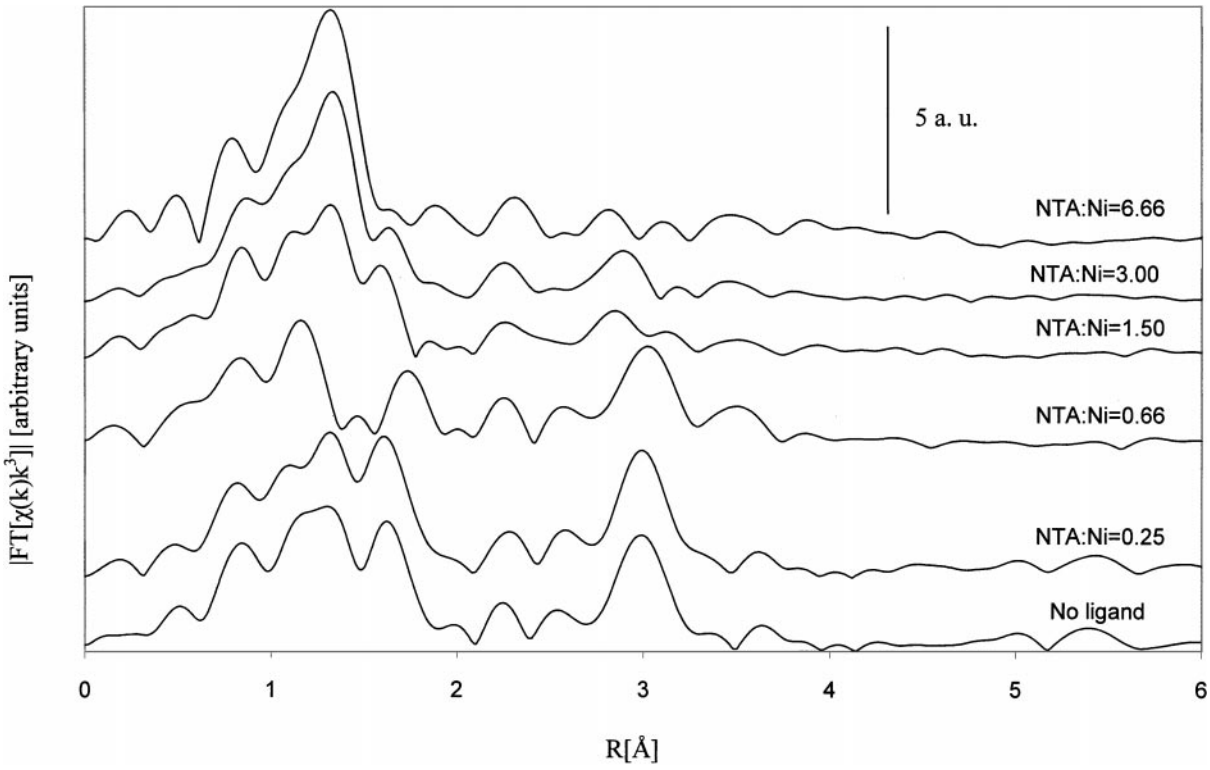

FIG. 10. Absolute parts of the Fourier transforms of the Mo *K*-edge $\chi(k) \cdot k^3$ EXAFS of dried $NiMo/SiO_2$ catalyst precursors as a function of the amount of nitrilotriacetic acid used during preparation (*k*-range 3–17 $Å^{-1}$).

Mo–Mo contributions was carried out and gave 0.5 and 0.4 Mo neighbor atoms at a distance of 3.16 and 3.42 Å, respectively, typical Mo–Mo distances in $Mo_7O_{24}^{6-}$ clusters. A similar split was observed in the k^3-weighted EXAFS spectrum of $(NH_4)_6Mo_7O_{24}$ simulated with the Feff7 code. The reference for the Mo–Mo shell was taken from the experimental Mo–Mo EXAFS contribution in MoS_2.

Mo XAS of NiMoNTA/SiO₂. The features of the Mo *K*-edge Fourier transformed k^3-weighted EXAFS functions of $NiMoNTA/SiO_2$ catalyst precursors, plotted in Fig. 10, demonstrate how Mo is affected by the presence of the chelating ligand. To understand the changes caused by the increasing NTA concentrations, it must be taken into account that the formation of the $[MoO_3(NTA)]^{3-}$ complex is possible only when NTA is present at NTA/Ni ratios higher than one, because NTA is much more strongly bonded by Ni^{2+} than by Mo^{6+} (1).

The Mo–Mo contribution at 3 Å (not phase-corrected) is reduced drastically when the NTA/Ni ratio is increased from 0.66 to 1.5. As can be seen from the spectra of the catalyst precursors with NTA/Ni = 0.25 and 0.66, Mo does not react to the presence of the chelating agent, and some polymolybdate is still present on the support. In the three cases in which a Mo–Mo contribution at 3 Å is observed, the Mo–Mo coordination number is always around 1.1. In the spectra of the three catalyst precursors with NTA/Ni ratios higher than 1, a new weak signal around 2.8 Å is observed. Its intensity was too low to carry out a significant fit, however.

DISCUSSION

The beneficial effect of chelating ligands during wet catalyst preparation on HDS catalytic activity is not limited to mixed amino–acetic acid-containing complexes such as NTA and EDTA. Amines, crown ethers and organic acids also improve activity. However, ligands with the largest number of coordinating atoms (NTA, EDTA, PT, citric acid) have the strongest effect. The ligand/Ni ratio was 1 in all cases. For NTA and EDTA this means that Ni, but not Mo, is coordinated by the ligands (1). The Mo *K*-edge EXAFS showed that this is also true for EN (Fig. 9). This is likely to be the case for the other amine ligands as well, since Ni forms very stable complexes with these ligands (Table 1). These observations indicate that *better protection* of the nickel ions in the catalyst precursors enables the preparation of more active catalyst. UV-VIS results showed that, in the absence of ligands, the ammonia molecules in the first coordination shell of Ni are substituted by oxygen atoms. This is due to the evaporation of NH_3 during the drying procedure, leaving behind Ni ions that are

exclusively coordinated by oxygen atoms from H_2O, OH^-, O^{2-}, or SiO^- (1). This was confirmed by the Ni *K*-edge EXAFS data, which clearly showed a Ni–Si interaction. In fact, the Ni–Si coordination number of 4.5 suggests that Ni is either adsorbed on the surface or built in the SiO_2 frame in a tetrahedral position, since the Ni–O coordination number is also close to 4.

For the dried EN-containing catalyst precursors, UV–VIS and EXAFS showed that EN could be removed from the Ni^{2+} ions as well. The EXAFS curve fittings indicated that Ni^{2+} has no carbon neighbor in the catalyst precursors when EN/Ni = 0.16 and 0.66, about two carbon neighbors when EN/Ni = 3.33 and probably six carbon neighbors in the dried catalyst precursor with the highest EN amount. The reason for the decrease in EN molecules coordinated to Ni^{2+} is again the exchange of ligand molecules for oxygen atoms of the support. Bonneviot *et al.* observed the same phenomenon for Ni/SiO_2 samples prepared from $[Ni(NH_3)_6]^{2+}$ by ion exchange (24). Burattin *et al.* used the deposition precipitation method to deposit Ni^{2+} on SiO_2 (4, 5). According to these authors, the Ni(II) hydroaqua complexes close to the silica surface can react with the silanol groups via an hydrolytic adsorption. They suggest that a Ni phyllosilicate layer forms on the support with subsequent stacking. We concluded from EXAFS spectroscopy that, in the absence of ligands, nickel is present almost exclusively as nickel silicate. EN inhibits the formation of nickel silicates, because the chelating diamine molecules prohibit hydrolytic adsorption on the support. Nevertheless, UV–VIS spectroscopy demonstrates that a fraction of EN coordinated to Ni^{2+} is removed during drying and is substituted by oxygen atoms of the support. The EN/Ni ratio must be substantially higher than 6 to ensure that all the Ni is coordinated by three EN molecules.

NTA behaved differently to EN. Ni–Si interactions were observed only at the lowest NTA concentration, whereas in catalyst precursors containing larger amounts of NTA, Ni is present as isolated ions on the support. This can be explained by the fact that EN has only two binding sites, whereas NTA has four and forms much more stable complexes with Ni than does EN, protecting Ni better and hindering interactions with the support. For this reason, the activity of catalysts prepared with NTA is much more dependent on the ligand concentration for NTA/Ni ratios below 1. Even for this chelating ligand the amount needed to keep all Ni fully coordinated by NTA is considerably higher than the expected ligand/Ni ratio of 1. The formation of $[Ni(NTA)_2]^{4-}$ would also be possible with larger amounts of NTA. However, the complex with only one ligand molecule seems to be the species present on the support, since in $[Ni(NTA)_2]^{4-}$ Ni would have eight neighboring carbon atoms, whereas the Ni–C coordination number obtained from the fit of the spectrum of the precursor catalyst with NTA/Ni = 6.66 was only 5.9.

The addition of ligand molecules causes the complexation of the Ni ions, and the number of Ni support connections decreases. We could show that, as far as silica is concerned, the weaker the Ni–SiO_2 interactions in the catalyst precursor are, the higher the catalytic activity of the eventual catalyst is. In fact, the absence of links with the support enables better mobility of Ni on SiO_2 so that, during sulfidation, it can easily move closer to the MoS_2 and form the Ni–Mo–S phase. The presence of the ligand, meanwhile, delays the sulfidation of Ni and subsequent formation of Ni_3S_2 (12, 15).

Raman spectroscopy indicates the presence of two different Mo species, $Mo_7O_{24}^{6-}$ and isolated MoO_4^{2-}. The Mo–Mo coordination number of the catalyst precursor without a ligand, as determined by EXAFS, is 0.9. Considering the fact that, in an heptamolybdate polyanion, the average Mo–Mo coordination number is 3.4, the fraction of Mo atoms in the clusters is about one-third of the total Mo present on the support surface. The main Mo species present is, therefore, MoO_4^{2-}. EXAFS revealed no evidence of a Mo–support interaction, as was indicated by Raman spectroscopy. EN does not seem to have a significant effect on the structure of the Mo compounds on the support. NTA, on the other hand, has a dramatic effect on the structure of Mo when it is present at NTA/Ni ratios higher than 1. Mo then forms the complex $[MoO_3(NTA)]^{3-}$. Since the Ni/Mo molar ratio is 0.3/1, all Mo will be complexed by NTA only when NTA/Ni $\cong$ 4.3. We conclude from the Mo *K*-edge spectrum of the catalyst precursors with NTA/Ni = 1.5 that the first effect of NTA is that polymolybdate clusters are not formed, since a Mo–Mo contribution was not observed.

The catalytic activity of catalysts prepared with NTA decreases for NTA/Ni ratios higher than 2. At this NTA concentration, about one-third of the Mo atoms should be complexed with NTA. The further decrease in catalytic activity corresponds to the gradual complexation of Mo, suggesting that NTA has a negative effect on the performance of the catalysts when it interacts with Mo. In fact, the presence of NTA can delay the formation of MoS_2 crystallites, so that at the temperature at which the MoS_2 crystallites are formed, Ni has already reacted to Ni_3S_2 and can not join the MoS_2 edges and constitute the active sites (15).

CONCLUSIONS

Catalytic tests in the hydrodesulfurization of thiophene at atmospheric pressure showed that a wide variety of organic ligands have a beneficial effect on the catalytic activity of NiMo catalysts supported on SiO_2. The activity of catalysts prepared with EN and NTA exhibited a significant improvement with ligand/Ni ratios between 0 and 4 for EN and from 0 to 1.5 for NTA, suggesting that Ni is responsible for the increase in catalytic activity. A decrease in the activity was observed for higher ligand concentrations.

The increase in activity is explained by the elimination of Ni–support interactions obtained by the addition of the ligands. In the case of catalyst precursors prepared with EN, EXAFS reveals a Ni–Si shell until EN/Ni = 3.3, whereas NTA eliminates such interactions already at NTA/Ni lower than 0.66. For these reasons the activity profile of catalysts prepared with EN shows a slower increase with respect to the ligand concentration. Moreover, UV–VIS spectroscopy showed that part of the EN is removed from the Ni environment during the drying procedure.

Raman spectroscopy and Mo *K*-edge EXAFS both showed that Mo is present on the support as a mixture of MoO_4^{2-} and polymolybdate clusters, the former being the main species. Raman spectroscopy suggests, furthermore, the presence of polymolybdate clusters interacting with the support. Fourier-filtered Mo *K*-edge EXAFS spectra of the samples containing different amounts of EN and NTA showed that EN has hardly any effect on Mo, whereas for NTA concentrations higher than 1 $[MoO_3(NTA)]^{3-}$ is formed. The formation of this complex has a negative effect on the performance of the catalysts as the decrease in catalytic activity of catalysts with NTA/Ni ratios higher than 2 showed.

More detailed information about the effects of chelating ligands can be found by following the changes in Ni and Mo during the sulfidation process (15).

ACKNOWLEDGMENTS

The authors thank the Swiss Norwegian Beamline staff for assistance during the EXAFS measurements at ESRF and C. Stinner and P. Fabrizioli of the Laboratory of Technical Chemistry of the ETH Zürich for the Raman and UV–VIS measurements. This work was supported by the Swiss National Foundation.

REFERENCES

1. Medici, L., and Prins, R., *J. Catal.* **163**, 28 (1996).
2. Williams, C. C., Ekerdt, J. G., Jehng, J., Hardcastle, F. D., Turek, A. M., and Wachs, I. E., *J. Phys. Chem.* **95**, 8781 (1991).
3. Bañares, M. A., Hu, H., and Wachs, I. E., *J. Catal.* **155**, 249 (1995).
4. Burattin, P., Che, M., and Louis, C., *J. Phys. Chem. B* **101**, 7060 (1997).
5. Burattin, P., Che, M., and Louis, C., *J. Phys. Chem. B* **102**, 2722 (1998).
6. Louis, C., Cheng, Z. X., and Che, M., *J. Phys. Chem.* **97**, 5703 (1993).
7. Thompson, M. S., European patent application, 01.181.035.A2 (1986).
8. van Veen, J. A. R., Gerkema, E., van der Kraan, A. M., and Knoester, A., *J. Chem. Soc. Chem. Commun.* **1987**, 1684 (1987).
9. Louwers, S. P. A., and Prins, R., *J. Catal.* **133**, 94 (1992).
10. Hiroshima, K., Mochizuchi, T., Honma, T., Shimizu, T., and Yamada, M., *Appl. Surf. Sci.* **121/122**, 433 (1997).
11. Inamura, K., Uchikawa, K., Matsuda, S., and Akai, Y., *Appl. Surf. Sci.* **121/122**, 468 (1997).
12. Medici, L., and Prins, R., *J. Catal.* **163**, 38 (1996).
13. Candia, R., Sørenson, O., Villadsen, J., Topsøe, N. Y., Clausen, B. S., and Topsøe, H., *J. Phys. Chem.* **95**, 123 (1991).
14. Eijsbouts, S., *Appl. Catal. A* **158**, 53 (1997).
15. Cattaneo, R., Shido, T., and Prins, R., to be published.
16. Pascarelli, S., Boscherini, F., D'Acapito, F., Hardy, J., Meneghini, C., and Mobilio, S., *J. Synchrotron Rad.* **3**, 147 (1996).
17. Kampers, F. W. H., Maas, T. M. J., van Grondelle, J., Brinkgreve, P., and Koningsberger, D. C., *Rev. Sci. Instrum.* **60**, 2635 (1989).
18. van Zon, J. B. A. D., Koningsberger, D. C., van 't Blik, H. F. J., and Sayers, D. E., *J. Chem. Phys.* **82**, 5742 (1985).
19. Kirlin, P. S., van Zon, F. B. M., Koningsberger, D. C., and Gates, B. C., *J. Phys. Chem.* **94**, 8439 (1990).
20. Lytle, F. W., Sayers, D. E., and Stern, E. A., *Physica B* **158**, 701 (1989).
21. Zabinsky, S. I., Rehr, J. J., Ankudinov, A., Albers, R. C., and Eller, M. J., *J. Phys. Rev. B* **52**, 2995 (1995).
22. "Gmelin Handbook of Inorganic Chemistry." Springer Verlag, 1989.
23. Larson, S. B., Simonsen, S. H., Ramsden, J. N., and Lagowski, J. J., *Acta Crystallogr.* **C45**, 161 (1989).
24. Bonneviot, L., Legendre, O., Kermarec, M., Olivier, D., and Che, M., *J. Colloid Interface Sci.* **134**, 534 (1990).
25. Martell, A. E., and Motekaitis, R. J., "The Determination and Use of Stability Constants." VCH, New York, 1988.
26. Smith, R. M., and Martell, A. E., "Critical Stability Constants." Plenum, New York, 1989.
27. Garcia-Granda, S., and Gomez-Beltran, F., *Acta Crystallogr.* **C40**, 1145 (1984).
28. Clause, O., Kermarec, M., Bonneviot, L., Villain, F., and Che, M., *J. Am. Chem. Soc.* **114**, 4709 (1992).
29. Greenwood, N. N., and Earnshaw, A., "Chemistry of the Elements." Pergamon, New York, 1986.
30. Williams, C. C., Ekerdt, J. G., Jehng, J., Hardcastle, F. D., and Wachs, I. E., *J. Phys. Chem.* **95**, 8791 (1991).
31. Griffith, W. P., and Lesniak, P. J. B., *J. Chem. Soc. A*, 1066 (1969).
32. Tytko, K. H., and Schonfeld, B. Z., *Z. Naturforsch.* **30B**, 471 (1975).
33. Gonzales-Vilchez, F., and Griffith, W. P., *J. Chem. Soc. Dalton Trans.* **1972**, 1416 (1972).
34. Jeziorowski, H., and Knözinger, H., *J. Phys. Chem.* **83**, 6642 (1980).
35. Payen, E., Grimblot, J., and Kasztelan, S., *J. Phys. Chem.* **91**, 6642 (1987).
36. Hardcastle, F. D., and Wachs, I. E., *J. Raman Spectrosc.* **21**, 683 (1990).
37. Kisfaludi, G., Leyrer, J., Knözinger, H., and Prins, R., *J. Catal.* **130**, 192 (1991).